Dynamics of a passively mode-locked semiconductor laser subject to dual-cavity optical feedback

Lina Jaurigue,[1] Oleg Nikiforov,[2] Eckehard Schöll,[1] Stefan Breuer,[2] and Kathy Lüdge[1,3]
[1]*Institut für Theoretische Physik, Sekr. EW 7-1, Technische Universität Berlin, Hardenbergstrasse 36, 10623 Berlin, Germany*
[2]*Institute of Applied Physics, Technische Universität Darmstadt, Schlossgartenstrasse 7, 64289 Darmstadt, Germany*
[3]*Department of Physics, Freie Universität Berlin, Arnimallee 14, 14195 Berlin, Germany*
(Received 2 October 2015; published 5 February 2016)

We study the influence of dual-cavity optical feedback on the emission dynamics and timing stability of a passively mode-locked semiconductor laser using a delay differential equation model and verify the timing stability results by an initial experiment. By bifurcation analysis in dependence of the feedback delay times and feedback strength bistability, quasiperiodic and chaotic dynamics, as well as fundamental mode-locking are investigated, yielding a comprehensive overview on the nonlinear emission dynamics arising due to dual-cavity optical feedback. Optimum self-locking ranges for improving the timing stability by dual-cavity optical feedback are identified. A timing jitter reduction and an increase of the repetition rate tuning range of up to a factor of three, compared with single-cavity feedback, are predicted for the parameter ranges investigated. Improved timing stability on short and long timescales is predicted for dual-cavity feedback through the suppression of noise-induced fluctuations. Based on the numerical predictions, experimentally, a maximum timing jitter reduction up to a factor of 180 is found, accompanied by a side-band reduction by a factor of 58 dB, when both feedback cavities are resonant.

DOI: 10.1103/PhysRevE.93.022205

I. INTRODUCTION

Passively mode-locked semiconductor lasers have been the subject of extensive research over the past 30 years [1–14]. This has been motivated by the wide range of potential applications, including optical data communication, optical clocking, and nonlinear microscopy [15–17]. A substantial portion of this research has gone into overcoming the large temporal pulse train instabilities, compared to solid-state lasers. Passively mode-locked semiconductor lasers exhibit large fluctuations in the arrival times between pulses, referred to as timing jitter, due to the absence of an external reference clock. Methods of reducing the timing jitter, that have been investigated thus far, include optical feedback, optical injection, and hybrid mode-locking. Hybrid mode-locking involves the external modulation of the absorber bias voltage. If the frequency of this modulation is within a certain range of the repetition rate of the mode-locked pulses a reduction in the timing jitter can be observed due to the imposed external frequency [18]. In the optical injection experiments, continuous wave light was injected into a passively mode-locked laser. Using this technique, timing jitter reduction and repetition rate tuning, which is important for compensating for cleaving tolerances when a precise repetition rate is required, has been achieved within a small locking range of the injected laser frequency [19]. Optical injection, however, has the disadvantage that a second laser is required, making the technique expensive and the setup more complicated. Optical feedback has been proven to be an effective means of timing jitter reduction [4–6,20,21], and has the advantage that no external modulation or injection source is needed.

In this work we study the influence of optical feedback, with a second optical fine-tunable feedback cavity, on the nonlinear emission dynamics of a two-section passively mode-locked laser. This is motivated by the frequency pulling that is observed for short feedback cavities and the timing jitter reduction that can be achieved with long feedback cavities [14]. We investigate the dynamics of such a system numerically, including repetition rate tunability, using a delay differential equation model. Subsequently, timing jitter reduction is investigated both theoretically and by an initial experiment.

This paper is divided into the following sections. In Sec. II we introduce the model used to study this system. In Sec. III we present results of numerical simulations, then in Sec. IV experimental results are presented. Conclusions are presented in Sec. V.

II. DELAY DIFFERENTIAL EQUATION MODEL

Based on the model proposed in Refs. [8,22], we model the passively mode-locked laser using a two-section ring cavity described by a set of three delay differential equations. The optical feedback and laser configuration considered in the model is depicted schematically in Fig. 1(a). The ring cavity geometry is used to be able to simplify the differential equations used to describe semiconductor passively mode-locked lasers. Despite the difference in geometry this model can be used to gain an understanding of the dynamics of a Fabry-Perot cavity mode-locked laser [Fig. 1(b)], as the dynamics are primarily determined by the total gain and losses integrated over the gain and absorber sections. Optical feedback is introduced by coupling the laser cavity to two passive feedback cavities. Dual cavity feedback is included in the delay differential equation model in the same manner as single-cavity feedback in Refs. [9] and [10]. A detailed description and derivation of the model with one feedback cavity can be found in Ref. [9]. The final set of three coupled delay differential equations is

$$\gamma^{-1}\dot{\mathcal{E}}(t)+\mathcal{E}(t)=R(t-T)e^{-i\Delta\Omega T}\mathcal{E}(t-T)+\sqrt{D}\xi(t)+\sum_{l=1}^{\infty}K_l k e^{ilC_1}R(t-T-l\tau_1)e^{-i\Delta\Omega(T+l\tau_1)}$$

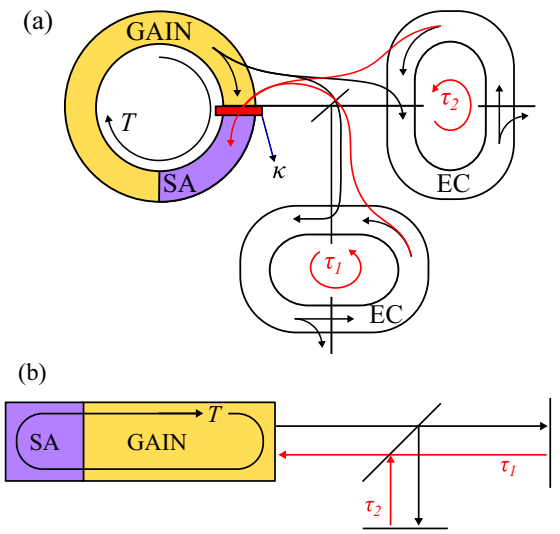

FIG. 1. Schematic of the dual-cavity optical feedback configuration studied numerically. (a) Ring cavity laser subject to optical feedback from two external cavities (EC). (b) Fabry-Perot laser cavity subject to optical feedback from two external cavities.

$$\times \mathcal{E}(t-T-l\tau_1) + \sum_{l=1}^{\infty} K_l(1-k)e^{ilC_2} \times R(t-T-l\tau_2)e^{-i\Delta\Omega(T+l\tau_2)}\mathcal{E}(t-T-l\tau_2), \tag{1}$$

$$\dot{G}(t) = J_g - \gamma_g G(t) - e^{-Q(t)}(e^{G(t)}-1)|\mathcal{E}(t)|^2, \tag{2}$$

$$\dot{Q}(t) = J_q - \gamma_q Q(t) - r_s e^{-Q(t)}(e^{Q(t)}-1)|\mathcal{E}(t)|^2, \tag{3}$$

with

$$R(t) \equiv \sqrt{\kappa}e^{\frac{1}{2}[(1-i\alpha_g)G(t)-(1-i\alpha_q)Q(t)]}. \tag{4}$$

The dynamical variables are the slowly varying electric field amplitude $\mathcal{E}$, the saturable gain G, and the saturable loss Q. The saturable gain G and saturable loss Q are related to the carrier inversion in the gain and absorber sections, respectively [9]. In Eq. (2), J_g is the excess (above transparency) current pumped into the gain section and J_q in Eq. (3) is the unsaturated absorption, which is related to the carrier losses due to the reverse bias applied to the absorber section. The carrier lifetimes in the gain and absorber sections are given by $1/\gamma_g$ and $1/\gamma_q$, respectively. The factor r_s is proportional to the ratio of the saturation energies in the gain and absorber sections. The three delay times in this system are the cold cavity round-trip time T and the external cavity round-trip times (delay time) τ_1 and τ_2. The cold cavity round-trip time is defined as $T \equiv v/L$, where L is the length of the ring cavity. The bandwidth of the laser is limited by the finite width of the gain spectrum, which is taken into account by a Lorentzian-shaped filter function with full-width at half maximum γ. The possibility of detuning between the frequency of the maximum of the gain spectrum and the frequency of the nearest cavity mode is allowed for by the inclusion of $\Delta\Omega$. The optical feedback is described by the two sums in Eq. (1). Here l is the number of round trips in the external cavity, K_l is the round-trip-dependent feedback strength and C_1, C_2 are the phases of the light due to one round trip in the external cavities. $K_l = K_l^1 + K_l^2$ is the total feedback strength from both external cavities, the contribution from each cavity is determined by k, $K_l^1 = kK_l$, and $K_l^2 = (1-k)K_l$. Under the assumption of weak feedback, we will consider feedback contributions only from light that has made one round trip in the feedback cavities ($l = 1$, $K_1 = K$). Spontaneous emission is modeled in Eq. (1) by a complex Gaussian white-noise term $\xi(t)$ with strength D.

TABLE I. Parameter values used in numerical simulations, unless stated otherwise.

Parameter	Value	Parameter	Value	Parameter	Value
γ	2.66 ps^{-1}	κ	0.1	T	50 ps
γ_g	1 ns^{-1}	α_g	0	D	0
γ_q	75 ns^{-1}	α_q	0	k	0.5
J_g	0.04 ps^{-1}	r_s	25	C_1	0
J_q	0.15 ps^{-1}	$\Delta\Omega$	0	C_2	0

Equation (4) describes the amplification and losses of the electric field $R(t)$ during one round trip in the ring cavity. Internal and out-coupling losses are taken into account in the attenuation factor κ and the line-width enhancement factor (α factor) in the gain and absorber sections are denoted α_g and α_q, respectively.

In the following, parameter values used will be those given in Table I, unless stated otherwise. The laser cavity round trip used here, $T = 50$ ps, corresponds to a 2-mm Fabry-Perot cavity. Additionally, in what follows we will refer to feedback cavity one as the long feedback cavity and feedback cavity two as the short feedback cavity, meaning $\tau_1 > \tau_2$.

III. SIMULATION RESULTS

A. Emission dynamics of a passively mode-locked laser subject to dual-cavity optical feedback

Passively mode-locked two-section lasers, when operated in the fundamental mode-locking regime, produce pulses of light due to a positive net gain window that opens once per cavity round trip. This positive net-gain window arises due to the absorber section saturating faster than the gain section [8,9]. Figure 2(a) shows a time trace depicting this behavior. Plotted in orange is the electric field amplitude and in black is the net gain. This time trace depicts the simulated output of a 20 GHz laser in the fundamental mode-locking regime. 20 GHz corresponds to a cold cavity round-trip time T of approximately 50 ps. The time between the pulses, referred to as the interspike interval time T_{ISI}, is slightly longer than T, as for the solitary laser $T_{\mathrm{ISI},0} \approx T + \gamma^{-1}$ [8]. The small positive net gain window coincides with the pulse, in between pulses the net gain is negative.

The dynamics of the passively mode-locked laser subject to optical feedback depends critically on the feedback strength and feedback delay time. For weak to moderate feedback from a single external cavity, resonant feedback can be achieved when

$$p\tau = qT_{\mathrm{ISI},0}, \tag{5}$$

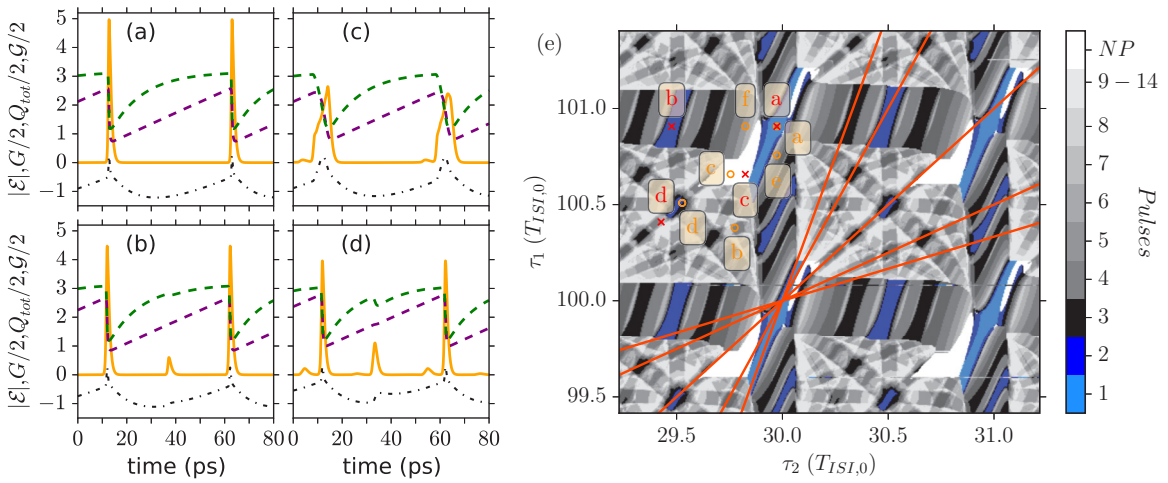

FIG. 2. (a)–(d) Calculated time traces of the electric-field amplitude (orange), the gain (dashed purple), the total losses $Q + |\ln\kappa|$ (dashed green), and the net gain $G - Q - |\ln\kappa|$ (dash-dotted black) for τ_1 and τ_2 values indicated by the red crosses in subplot (e). (e) Number of pulses in the laser cavity as a function of τ_1 and τ_2. NP indicates nonperiodic dynamics. Parameters: $J_g = 0.08\ \mathrm{ps}^{-1}$, $J_q = 0.3\ \mathrm{ps}^{-1}$, $K = 0.2$, other parameters as given in Table I.

for $p,q \in \mathbb{N}$ [9]. The integer p indicates the order of the resonance and the number of pulses within the laser cavity. For main resonant feedback ($p = 1$) the arrival times of the pulses, from the laser cavity and the feedback cavity, at the out coupling facet of the laser cavity coincide; hence, there is just one pulse within the laser cavity. About the main resonances there is a range of τ values for which self-locking occurs between the pulses traveling in the laser and feedback cavities. Within this self-locking range T_{ISI} adapts such that the arrival times of pulses at the laser out coupling facet are synchronized. For higher-order resonant feedback, small feedback-induced pulses travel within the laser cavity, along with the main pulse. For dual-cavity optical feedback, studied here, the same resonance condition [Eq. (5)] applies, however, now it must hold for both feedback cavities, and the number of pulses within the laser cavity has to be determined by a combination of p_1 and p_2. When the delay lengths of both feedback cavities fall within the main resonance self-locking ranges, there is one pulse within the laser cavity. This situation is depicted in the time trace of Fig. 2(a), where $\tau_1 \approx 100T_{\mathrm{ISI},0}$ and $\tau_2 \approx 30T_{\mathrm{ISI},0}$. In Fig. 2(b) the long cavity is at a main resonance and the short cavity is at a second-order resonance ($\tau_1 \approx 100T_{\mathrm{ISI},0}$ and $2\tau_2 \approx 59T_{\mathrm{ISI},0}$). This means that pulses from the short cavity arrive at the out coupling facet of the laser in between internal pulses, causing the small pulse that can be seen in the time trace. A key difference between the main pulses and the feedback induced pulses is that the latter are not sustained by a positive net-gain window. The net-gain profile is, however, altered by the feedback-induced pulses.

To gain a more complete picture of the feedback-delay dependence of the laser dynamics Fig. 2(e) shows the number of pulses in the laser cavity as a function of τ_1 and τ_2. The number of pulses is indicated by the color code. Regions in white, labeled NP, indicate a nonperiodic output. In these regions the laser can exhibit quasiperiodic or chaotic dynamics. The time traces in Figs. 2(a)–2(d) correspond to Fig. 2(e) as indicated by the red crosses. For Fig. 2(c) the feedback is nonresonant; here the pulses are highly deformed and the pulse shape varies from one laser cavity round trip to the next. For Fig. 2(d) both delay times are in a higher-order resonance. Multiple feedback-induced pulses can be seen in between the main pulses. As both feedback cavities are contributing to these pulses, the net-gain profile is more distorted than in Fig. 2(b). The total number of pulses within the laser cavity that can be resolved depends on the pulse widths and the cold cavity round-trip time.

Figure 2(e) displays a periodic resonance structure. The structure is approximately periodic in τ_1 and τ_2, with a periodicity of $T_{\mathrm{ISI},0}$. The main resonances for the two delays occur at integer multiples of $T_{\mathrm{ISI},0}$. Where these individual main resonance regions overlap we find the overall main resonances for the dual feedback system. These regions are where self-locking occurs between the pulse in the laser cavity and the pulses in both external cavities, and hence, where there are no feedback-induced pulses, i.e., one pulse in the laser cavity indicated by the light blue color code. The main resonance self-locking regions have a long axis and a short axis. The width along the long axis is greater because in this direction pulses from both feedback cavities either arrive too early or too late and the system can adapt the T_{ISI} in the appropriate direction for self-locking to occur. However, along the short axis the pulses from one cavity arrive too early and from the other too late, meaning that synchronization cannot occur when the delays deviate much in this direction. Between the main resonances a starlike pattern is formed by lines connecting resonance regions. The slopes of these lines depend on the order of the resonances being connected. This is illustrated by the red lines. Here $\tau_1 = 100T_{\mathrm{ISI},0}$ and $\tau_2 = 30T_{\mathrm{ISI},0}$ is taken as the origin, the lines are then plotted with the slopes determined by p_1 and p_2. Line (1) connects the main resonance region with a first-order resonance in τ_1 and a third-order resonance in τ_2; therefore, the slope of this line is given by $p_2/p_1 = 3/1$. Accordingly, the slopes of the other lines are as indicated in the plot. Similar patterns are found in dependence of the delay times in systems of coupled neural oscillators [23].

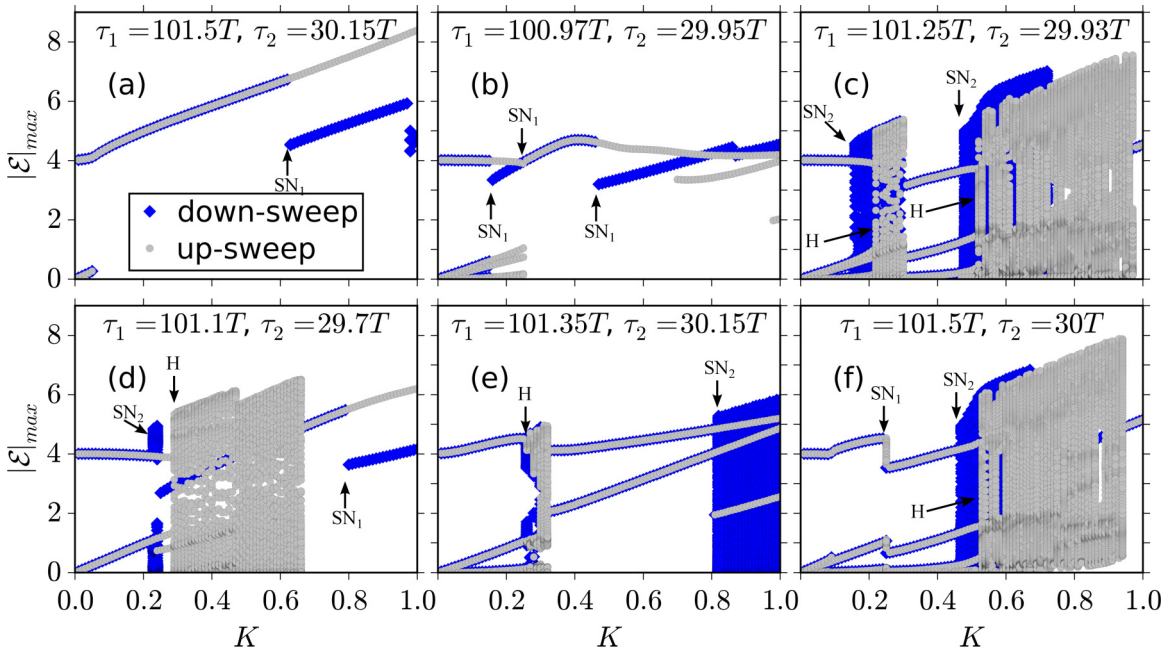

FIG. 3. Numerical bifurcation diagrams as a function of the total feedback strength K. Plotted on the y axes are electric field maxima collected over a time period of $100T$ for up-sweeps (gray circles) and down-sweeps (blue diamonds) of K. SN_1, SN_1, and H indicate the critical K values where saddle-node bifurcations of limit cycles, saddle-node bifurcations of quasiperiodic solutions, and subcritical secondary Hopf bifurcations occur, respectively. Parameters: $J_g = 0.08$ ps^{-1}, $J_q = 0.3$ ps^{-1}; other parameters as given in Table I.

For the results considered thus far the feedback strength was kept constant. However, as is the case with single-cavity feedback, the exhibited dynamics with dual feedback depend strongly on the feedback strength. For single-cavity feedback it was found that with increasing feedback strength the self-locking regions of the main resonances increase, whereas the self-locking regions of higher-order resonances decrease, forming a Farey treelike dependence [9]. And that, depending on the feedback delay time, increasing feedback strength can lead to quasiperiodic and eventually chaotic dynamics. To gain an understanding of the influence of the total feedback strength K on the dynamics in the dual feedback case, numerical bifurcation diagrams are shown in Fig. 3 as a function of K, for varying feedback delay times. Plotted on the y axes are maxima in the electric field output, i.e., pulse heights. These results were obtained by up-sweeping (gray cirles) and down-sweeping (blue diamonds) K. This means that the delay differential equation system [Eqs. (1)–(3)] was numerically integrated for sufficiently long times to avoid transient behavior, then $|\mathcal{E}|$ maxima were recorded for a simulation time of $100T$ and then the history of the current simulation was used as the initial conditions for the next K step. Here, only the total feedback strength is varied, the feedback ratio from the two cavities is kept constant ($k = 0.5$). The delay times in Figs. 3(a)–3(f) correspond to Fig. 2(e) as indicated by the cyan circles. For Fig. 3(a) the delay times are very close to the exact main resonance. For very small feedback strengths, up to $K \approx 0.08$, there are two pulses in the laser cavity, indicated by the markers at two different amplitudes. As the feedback strength is increased, the main resonance regions eventually extend to include the delay times used for this subplot. The K value at which this occurs is where the small feedback-induced pulse disappears. $K = 0.2$ is past this point, and accordingly the delay times used here lie within the main resonance region in Fig. 2(e). In the down-sweep direction a saddle-node bifurcation occurs at approximately $K = 0.6$, indicated by SN_1 in the figure. Above this point the fundamental mode-locked solution (upper solution) is bistable with the second harmonic mode-locked solution (lower solution).

For Fig. 3(b) the delay times were chosen to lie on the long axis of the $\tau_1 = 101T_{ISI,0}$, $\tau_2 = 30T_{ISI,0}$ main resonance in Fig. 2(e). The trend in this plot is similar to that of Fig. 3(a). For small feedback strengths there are multiple pulses, until the feedback strength is large enough that the main resonance self-locking regions extend to these delay times, after which there is a K range where there is only one pulse in the laser cavity. There is a region of bistability between the fundamental mode-locked solution and solution with multiple feedback-induced pulses, which is bordered by saddle-node bifurcations of the up- and down-sweep branches. Increasing K further, there is another saddle-node bifurcation of the down-sweep branch ($K \approx 0.45$), above which this branch is on the second harmonic mode-locked solution.

To understand what gives rise to the white nonperiodic regions in Fig. 2(e), the delay times for Fig. 3(c) are chosen in one of these regions. For small K the solutions are periodic, with multiple feedback-induced pulses. As K is increased, a subcritical secondary Hopf (Torus) bifurcation occurs just above $K = 0.2$ (indicated by H in the figure) and the solution jumps to a branch of quasiperiodic solutions. For higher K values the solution jumps back to a periodic mode-locked branch, followed by a second subcritical secondary Hopf bifurcation. The branches of unstable quasiperiodic solutions generated by the subcritical secondary Hopf bifurcations (not shown) undergo saddle-node bifurcations at the K values indicated by SN_2 in the figure.

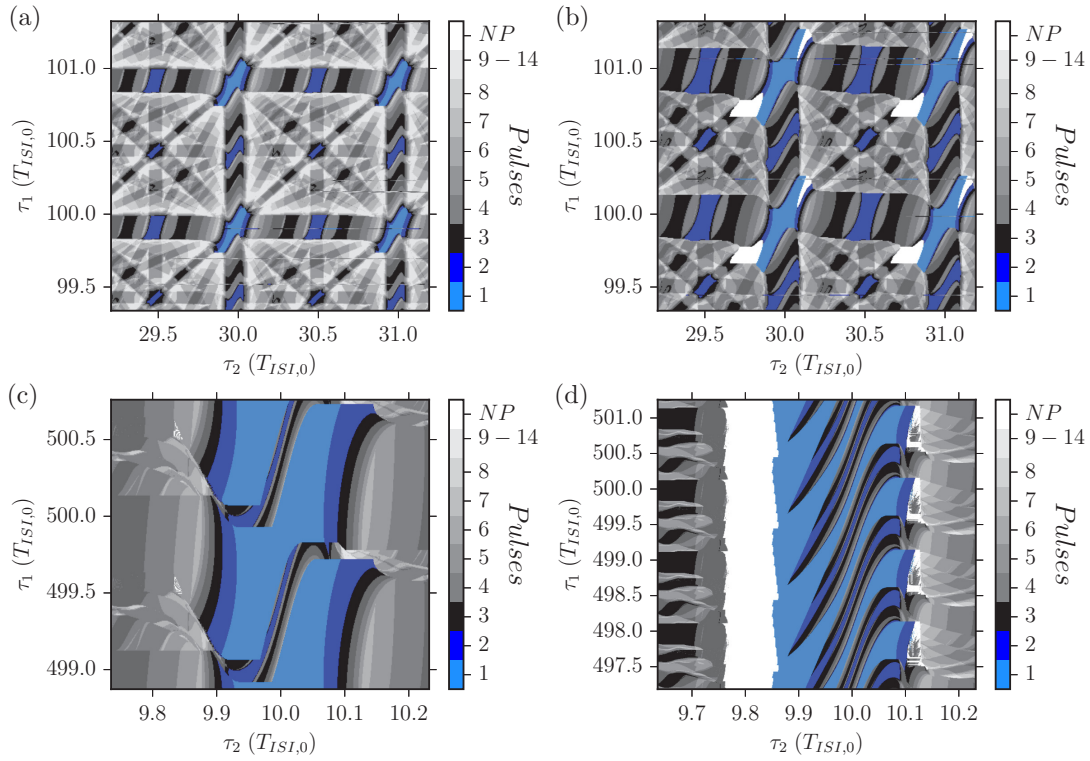

FIG. 4. Number of pulses in the laser cavity as a function of τ_1 and τ_2. NP indicates nonperiodic dynamics. Parameters: $K = 0.1$, (a) $J_g = 0.08$ ps^{-1} and $J_q = 0.3$ ps^{-1}, (d) $k = 0.2$; all other parameters as given in Table I.

Figure 3(d) shows the K dependence when both delay times correspond to a second-order resonance. For large K, after the system has gone through a subcritical Hopf bifurcation and the branch of quasiperiodic solutions has become unstable, in the range $K \approx 0.68$–0.8 there are no feedback-induced pulses. For these K values the delay times used here lie within the self-locking region of the $\tau_1 = 99T_{\mathrm{ISI},0}$, $\tau_2 = 29T_{\mathrm{ISI},0}$ main resonance.

Figures 3(a) and 3(b) have demonstrated that the main resonance self-locking regions increase along the long axis. To determine the behavior, with increasing K, along the short axis the delay times for Figs. 3(e) and 3(f) are chosen either side of the resonance region in Fig. 2(e), as indicated. From Figs. 3(e) and 3(f), one can deduce that the main resonance regions do not increase along the short axis, as there are no moderate K values for which the feedback-induced pulses disappear.

B. Optimization of resonant regions

For practical applications a wide resonance self-locking region is desirable. Figure 3 shows that the self-locking regions increase with the feedback strength; however, with increased K the dynamics can also become quasiperiodic or chaotic. The widths of the self-locking regions are also affected by various other parameters, including the feedback delay time and pulse widths. In Fig. 4 the pulse number is plotted, again as a function of τ_1 and τ_2, for various τ_1, τ_2, k, J_g, and J_q values. Figure 4(a) corresponds to Fig. 2(e), but with $K = 0.1$ instead of $K = 0.2$. Comparing these plots the change in the length of the main resonance region, with increasing K, can clearly be seen. In subplots (a) and (b) of Fig. 4, all parameters are the same except for J_g and J_q, which are reduced in subplot (b), resulting in wider pulses. The increased pulse width results in wider resonance self-locking ranges. Due to the wider self-locking ranges quasiperiodic dynamics, indicated by the white regions, appear at lower K values. Thus, also the operation parameters play a crucial role for the dynamics subject to feedback. In Fig. 4(c) the laser parameters are the same as in Fig. 4(b), here only the feedback delay times have been changed, τ_1 is of the order of 500, and τ_2 of the order of 10. Note that the depicted τ_2 range is smaller than in Fig. 4(a). The main resonance self-locking regions in Fig. 4(c) extend substantially further along the τ_1 axis than the τ_2 axis. We know that for single-cavity feedback the width of the main resonances increase for longer delay times [9]. This can be understood by considering the sychronization condition,

$$\tau = \tau_q + \delta\tau = qT_{\mathrm{ISI},0} + q\delta T_{\mathrm{ISI}}, \tag{6}$$

for self-locking between pulses in the laser and feedback cavities, where $\tau_q = qT_{\mathrm{ISI},0}$ is the delay time at the exact qth main resonance. When τ deviates from τ_q, the system must adapt T_{ISI} for self-locking to occur. The change in T_{ISI} is given by $\delta T_{\mathrm{ISI}} = \delta\tau/q$. For large q, smaller changes in the interspike interval time are required, hence the self-locking ranges are wider for longer delay times. (Note that the self-locking condition Eq. (6) is not strictly correct as it neglects changes in the pulse shape, which if included result in slightly smaller T_{ISI} changes.) For dual-cavity feedback the same principles apply, meaning that the self-locking ranges are greater for the long cavity compared to the short cavity. This is more obvious

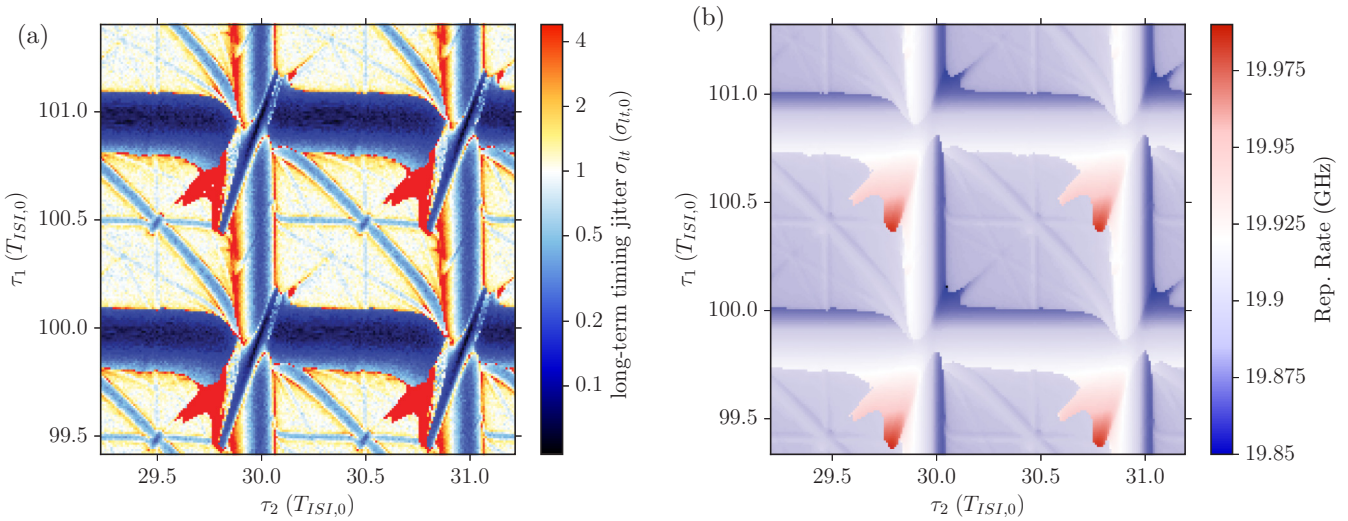

FIG. 5. (a) Calculated timing jitter as a function of τ_1 and τ_2. The timing jitter of the solitary laser is indicated by σ_{lt} of the color bar. (b) Repetition rate as a function of τ_1 and τ_2. Parameters: $J_g = 0.08$ ps^{-1}, $J_q = 0.3$ ps^{-1}, $K = 0.2$, $D = 3.2$ ns^{-1}; other parameters as given in Table I.

in Fig. 4(c), compared with Figs. 4(a) and 4(b), due to the increased difference in the cavity lengths.

An important feature of Fig. 4(c) is that along the τ_1 axis there is an overlap of main resonance regions, i.e., the width of the τ_1 main resonance is greater than the separation between main resonances, $T_{\text{ISI},0}$. This is a consequence of the difference in changes in T_{ISI} for long and short cavities. Over the τ_2 self-locking range, T_{ISI} changes from some minimum to some maximum value. For the same T_{ISI} range to be achieved with the long cavity, τ_1 needs to be varied over a much larger range. Thus, if the τ_2 self-locking range can be increased, then the τ_1 self-locking range increases accordingly. This situation is depicted in Fig. 4(d), where the relative feedback strengths have been changed such that the feedback from the short cavity is stronger, $k = 0.2$. Due to the increased feedback strength from the short cavity, the τ_2 self-locking range is increased slightly and the τ_1 self-locking range now spans over three main resonances. For single long cavity feedback the self-locking range can span over multiple $T_{\text{ISI},0}$; however, in this case there is a multistability between solutions locked to neighboring main resonances. Experimentally this typically leads to abrupt switching to different locked solutions as the delay is varied [3]. Adding an extra feedback cavity lifts this multistability. For applications these considerations mean that the accessible frequency pulling range, i.e., the tunable range of repetition rates, is larger in the dual feedback case than for a single long cavity.

C. Timing jitter reduction and frequency pulling

In the study of the dynamics of the mode-locked laser system, presented in the previous sections, no noise was included to account for the spontaneous emission that is present in experiments with lasers. Without noise the emission dynamics in the mode-locking regimes is perfectly regular. Introducing noise into the system causes fluctuations in the arrival times between pulses. These fluctuations are quantified by the timing jitter and are observed experimentally. For single-cavity feedback it has been shown that timing jitter reductions can be achieved under resonance conditions [10,13]. A physical explanation for the reduction in timing jitter is given in Ref. [14]. To investigate the influence of dual-cavity feedback on the timing jitter we calculate the timing jitter, using the long-term jitter method [10], in dependence of the feedback parameters. The long-term timing jitter σ_{lt} is related to the variance of the timing fluctuations, $\Delta t_n \equiv t_n - nT_C$, by

$$\sigma_{\text{lt}} \equiv \sqrt{\text{Var}(\Delta t_n)/n},$$

with $\text{Var}(\Delta t_n)(n,\tau) \equiv \langle[\Delta t_n(\tau)]^2\rangle_M$, where t_n is the arrival time of the nth pulse and T_C is the ideal interspike interval time [24]. We calculate the interspike interval time for $n = 40\,000$ round trips in the laser cavity and average over $M = 50$ noise realizations. Note that for a Gaussian white noise source the long-term jitter is directly proportional to the root mean square timing jitter calculated from the von Linde method [10,25].

In Fig. 5(a) the timing jitter is plotted as a function of τ_1 and τ_2. Regions in blue indicate a decrease in the timing jitter with respect to the free running laser. The yellow-red regions indicate an increase in the timing jitter. Aside from the noise strength, the same parameter values are used for Fig. 5(a) as were used for the deterministic results presented in Fig. 2(e). Comparing these two plots, timing-jitter reduction occurs in the main resonance self-locking regions, and in some of the higher-order resonant regions. The largest reduction in the timing jitter is achieved toward the center of the main resonance. The regions of destabilized pulse streams in Fig. 5(a) (dark-red regions indicating a large timing jitter) correspond to the nonperiodic regions of Fig. 2(e) (white regions). The influence of the feedback delay length on the timing jitter reduction can clearly be seen in this plot. In the first-order resonant regions of τ_1 the timing-jitter reduction is greater than in the first-order resonant regions of the smaller delay time τ_2. In Fig. 5(b) the repetition rate, $1/T_{\text{ISI}}$, is plotted and it can be seen that changes in the repetition rate occur across the resonant regions. The largest deviations in the repetition rate occur along the long axis of the main resonant regions.

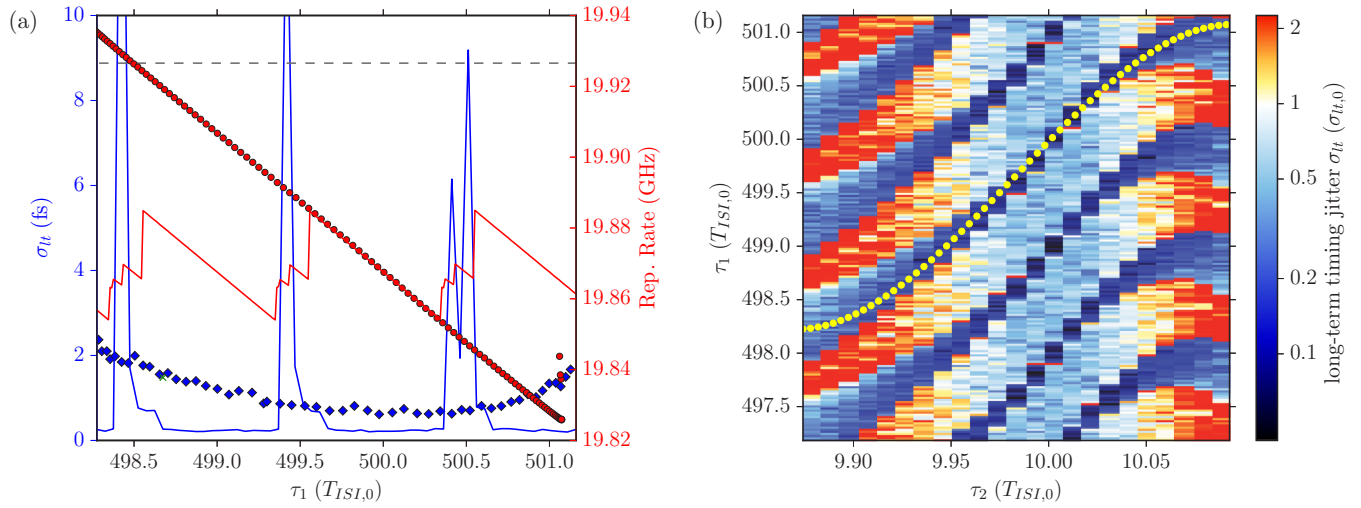

FIG. 6. (a) Calculated timing jitter (blue) and repetition rate (red) as a function of τ_1 for dual (markers) and single (solid lines) cavity feedback. The gray dashed line indicates the timing jitter of the solitary laser. (b) Timing jitter as a function of τ_1 and τ_2 for the dual feedback case. The yellow dotted line indicates the τ_1 and τ_2 values used in (a). Parameters: $K = 0.1$, $k = 0.2$, $D = 3.2$ ns^{-1}; other parameters as given in Table I.

As timing-jitter reduction and repetition-rate tuning can also be achieved with a single feedback cavity we compare the performance with the dual-cavity case. In Fig. 6(a) comparison of the long-term timing jitter and the repetition rate tuning is made between free-running operation, single- and dual-cavity feedback. In this case, $n = 120\,000$ round trips is used in the long-term timing jitter calculation, due to the increased length of the long cavity. Figure 6(a) shows the timing jitter in blue and the repetition rate in red, as a function of the long delay time (which in the case of single-cavity feedback is the only delay time). The solid lines show the results for single-cavity feedback and the markers depict the dual-cavity feedback results. The horizontal dashed gray line indicates the timing jitter of the solitary laser. For dual-cavity feedback the corresponding short-cavity delay times are indicated by the yellow dotted line in Fig. 6(b), in which the long-term timing jitter is plotted as a function of τ_1 and τ_2 for the parameter values corresponding to Fig. 4(d).

The single-cavity feedback results in Fig. 6(a) show timing jitter reduction at the main resonances (blue line). In between the main resonances there is a narrow τ range where the timing jitter is increased. These regions correspond to where the solution jumps from one main resonance self-locking region to the next. This can also be seen in the repetition rate (red line). Within one main resonance self-locking region there is an approximately linear change in the repetition rate, followed by sudden jumps at the transition between resonance regions. In the dual-cavity feedback case, through the addition of the short cavity, the τ_1 self-locking range for a main resonance is greatly increased. This is seen clearly by the linear change in the repetition rate over nearly the entire depicted τ_1 range (red markers), resulting in a three-fold increase in the repetition rate tuning range, as compared with single-cavity feedback. Over this entire range a substantial reduction in the timing jitter is also achieved (blue markers).

For the feedback parameters used in Fig. 6(a) the reduction of the long-term timing jitter is not as good in the dual-cavity feedback case as in the resonant single-cavity feedback case. Several factors contribute to this. First, for the comparison between single- and dual-cavity feedback the total feedback strength was chosen to be the same, $K = 0.1$, meaning that in the dual-cavity feedback case the contribution from the long cavity, which has the greatest effect on long-term timing jitter reduction, is only $Kk = 0.02$. If the feedback strength of the longer cavity is increased, better timing jitter reduction can be achieved. Second, the long-term timing jitter does not fully describe the timing stability of the system. It gives an indication of the timing stability over many thousands of round trips in the laser cavity, but contains no information on timing fluctuations on short timescales. However, short timescale fluctuations are important to consider when implementing optical feedback, as noise can excite resonant oscillations in the feedback cavities. These manifest themselves as periodic fluctuations in the amplitude and interspike interval time of the mode-locked pulses, the frequency of which is determined by the feedback delay time ($1/\tau$). The damping of such fluctuations depends on the feedback strength, the delay time, and, in the dual-cavity feedback case, on the length of the second cavity, as will be discussed next.

In Fig. 7(a) power spectra are shown for the single- and dual-cavity feedback cases corresponding to the delay times marked by the vertical dotted line in Fig. 6(a). The main peak in the spectra is at the repetition frequency of the pulsed output. The noise-induced resonant oscillations in the feedback cavities manifest themselves as peaks in the sidebands of the main peak. These can clearly be seen in the single-cavity feedback case (blue line). The separation of the side peaks is approximately $1/\tau \approx 40$ MHz. The presence of these side peaks means that the interspike interval time oscillates even though the long-term timing jitter is relatively small. In the dual-cavity feedback case these oscillations are suppressed due to the presence of the short cavity. The damping of these oscillations occurs because they are not resonant with the short cavity; i.e., the fundamental frequency of the short cavity

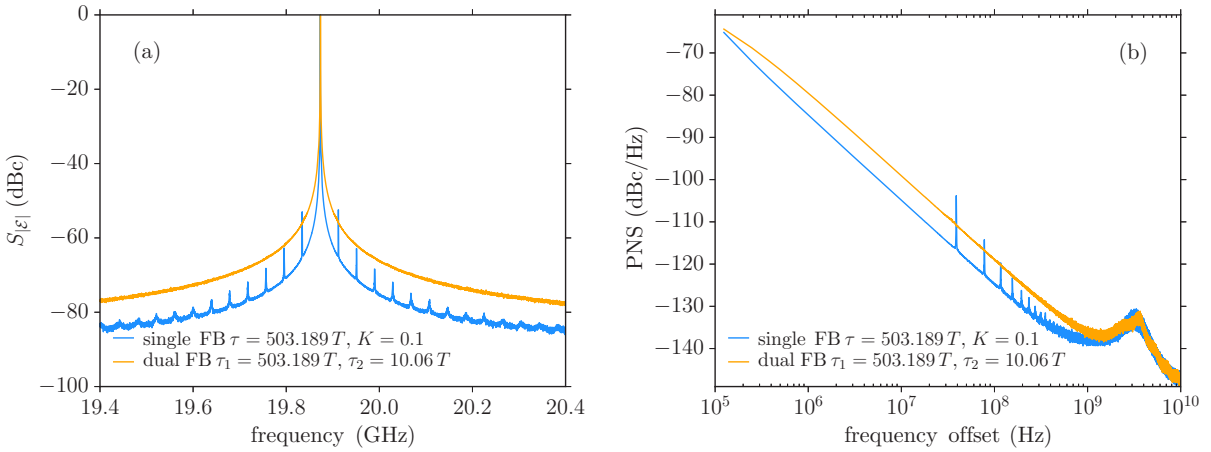

FIG. 7. (a) Calculated power spectrum for single-cavity (blue) and dual-cavity (orange) feedback. Parameters: $K = 0.1$, $k = 0.2$, $D = 12.8\ \mathrm{ns}^{-1}$; other parameters as given in Table I. (b) Extracted phase noise spectra from (a).

is $1/\tau_2 \approx 2$ GHz, which is much greater than the 40-GHz fundamental frequency of the long cavity. Therefore, the pulse train is more regular on short to intermediate timescales in the dual-cavity feedback case as compared with the single-cavity feedback case.

Depicted in Fig. 7(b) are the corresponding phase noise spectra. These are calculated from the power spectra in Fig. 7(a) by dividing them by the power integrated over the main peak. The frequency axis gives the offset from the main peak. In experiments, such as those discussed in the next section, the phase noise spectra are used to determine the root-mean-square timing jitter.

The dual-cavity configuration can be chosen in such a way that the long-term timing jitter reduction is greater than in the single long-feedback-cavity case. This is achieved by increasing the length of the short cavity and selecting a resonance that is not a factor of the long cavity. In such a configuration, the suppression of the resonant oscillations, combined with the increased contribution to the timing-jitter reduction from the short cavity (due to its increased length), leads to a lower long-term timing jitter than with a single long cavity with the same total feedback strength. This is verified numerically, e.g., for the single-cavity feedback case, with $\tau = 500\,T_{\mathrm{ISI}}$ and $K = 0.1$, $\sigma_{\mathrm{lt}} = 0.23$ fs is calculated and in the dual-cavity case, with $\tau_1 = 500\,T_{\mathrm{ISI}}, \tau_2 = 270\,T_{\mathrm{ISI}}, k = 0.5$ and $K = 0.1$, $\sigma_{\mathrm{lt}} = 0.18$ fs is calculated (all other simulation parameters as in Table I).

In the experimental results section following below, the predicted behavior of timing-jitter reduction and side-peak suppression with dual-cavity feedback are verified by an initial experimental investigation.

D. Influence of amplitude-phase coupling and feedback-phase dependence

In the results presented thus far the amplitude-phase coupling and feedback phase-shifts were set to zero. Here we address the influence of these parameters. Similar to the case of single-cavity feedback all the general behavior of the modeled mode-locked laser are the same when amplitude-phase coupling is included [10]. Figure 8 shows a map of the number of pulses in the laser cavity as a function of τ_1 and τ_2 for $\alpha_1 = \alpha_2 = 1$. We have chosen low values for the amplitude-phase coupling, as these are typical of quantum-dot materials [26–28], and in the following section experimental results for a quantum-dot mode-locked laser are presented. Comparing Fig. 8 with Fig. 2(e), the same general patterns are present, i.e., when both feedback cavities are resonant there is one pulse in the laser cavity and at higherorder resonances there can be multiple feedback-induced pulses. However, the main resonance self-locking regions are smaller and not as regular in shape and size. This is partly due to the phase sensitivity of the system. Due to the nonzero amplitude-phase coupling there is a carrier-induced shift in the optical frequency of the laser. This shift is affected by all laser and feedback parameters. Therefore, because Eqs. (1)–(3) are in the rotating frame of the carrier frequency for zero-amplitude phase coupling, there is a dynamical shift in the phase difference between the laser and feedback cavities, and this phase difference changes with τ_1 and τ_2.

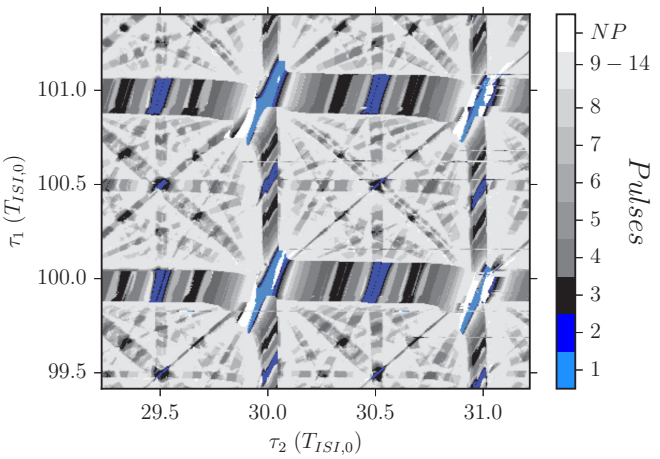

FIG. 8. Number of pulses in the laser cavity as a function of τ_1 and τ_2. NP indicates nonperiodic dynamics. Parameters: $J_g = 0.08\ \mathrm{ps}^{-1}$, $J_q = 0.3\ \mathrm{ps}^{-1}$, $\alpha_g = \alpha_q = 1$; all other parameters as given in Table I.

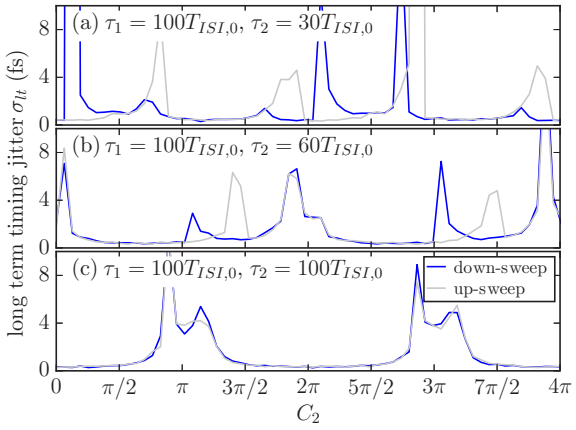

FIG. 9. Long-term timing jitter as a function of the feedback phase of the short cavity C_2, for up- and down-sweeps of C_2. Parameters: $J_g = 0.08$ ps^{-1}, $J_q = 0.3$ ps^{-1}, $\alpha_g = \alpha_q = 1$, all other parameters as given in Table I.

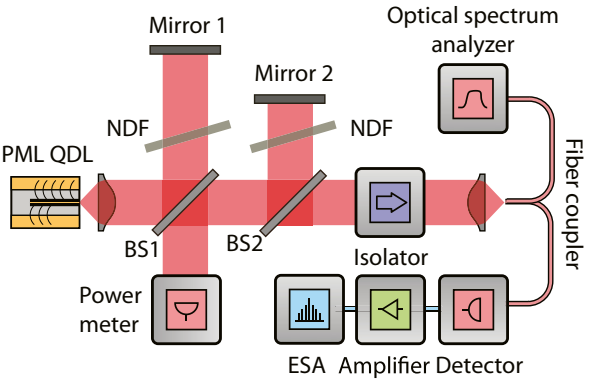

FIG. 10. Sketch of the experimental setup used to study the influence of dual-cavity optical on the timing jitter and emission dynamics of a two-section quantum dot mode-locked laser. BS1 and BS2, 50/50 beam splitters; M1 and M2, feedback mirrors; NDF, neutral density filters.

Figure 9 shows the timing jitter as a function of the feedback phase of the short cavity C_2 for up- and down-sweeps of the initial conditions. For all delay lengths depicted a clear phase dependence can be seen, changes in the phase over a range of 2π can lead to large increases in the timing jitter. Figures 9(a) and 9(b) also show hysteresis. As with single-cavity feedback the phase dependence seems to decrease with increasing feedback delay times [9]. In Fig. 9 this is shown by the increased C_2 ranges over which the timing jitter is constant as τ_2 is increased. However, the system appears to be more sensitive to the phases of the feedback cavities than in the single-cavity feedback case. Experimentally, this might make tuning the repetition rate difficult; however, as will be shown in the subsequent section, dual feedback configurations that lead to a substantial improvement in the timing jitter reduction can be found. It should also be noted that factors that lead to fluctuations in the feedback phases in an experiment can affect both feedback cavities. In Fig. 9 C_1 was kept constant. Changing both phases in some consistent way may led to improved results. Last, these results do not exclude the possibility of solutions or parameter regimes in which less phase sensitivity is exhibited, as the system is highly multistable and solutions found numerically depend strongly on the initial conditions.

IV. EXPERIMENTAL RESULTS

The passively mode-locked laser under investigation is a 2-mm-long two-section InAs/InGaAs quantum dot laser with a 10% absorber section and cleaved facets. The laser emits an optical pulse train with picosecond-short optical pulses at wavelengths around 1250 nm, with a repetition rate of 20 GHz, corresponding to the repetition rate of the simulated laser in the previous sections. The gain section current is 57 mA and a reverse-bias voltage of 4 V has been used. The developed experimental setup is depicted in Fig. 10. This setup allows for fine-delay tuning of both external cavity lengths. The laser light is collimated by an aspheric lens and a part of the beam is reflected by a 50/50 beam splitter (BS1) onto a mirror (M1), which is mounted on a fine-delay translation stage. The transmitted light is again split by a 50/50 beam splitter (BS2) and directed to the second mirror (M2), which is also mounted on a translation stage. The beam is directed through an optical isolator (60-dB isolation) to suppress possible back-reflections from the fiber coupling. Emission analysis is performed using a high-frequency photodetector (50 GHz) with an amplifier and electrical spectrum analyzer (50 GHz), and an optical spectrum analyzer (resolution 20 pm).

The chosen dual-cavity feedback delay lengths are 15.9 m for the short cavity and 33.4 m for the long cavity, which correspond to pulse round-trip frequencies of 9.4 and 4.5 MHz, respectively. The feedback strengths are 0.22 % of the output power for the short cavity and 1.7 % for the long cavity.

As in the simulations, the timing jitter is quantified by the long-term timing jitter σ_{lt}, which is calculated from the experimentally measured root-mean-square timing jitter σ_{rms}, for an integration range from 100 kHz to 1 GHz, according to Ref. [10]. The measured radio frequency spectra used for this, for free-running operation, short-cavity feedback, long-cavity feedback, and dual-cavity feedback, are depicted in Fig. 11(a). For the dual-cavity feedback measurement the fine-delay of each cavity was adjusted for maximum timing-jitter reduction. Comparing with the theoretical results, this corresponds to moving the operation point to the main resonance region. The single-cavity feedback measurements were then carried out with exactly the same delay lengths by blocking the light from the second cavity. As a first experimental measure to quantify the improvement of timing jitter, the line widths Δf of the measured power spectra are considered. In the free-running operation, a Lorentzian line shape is observed with $\Delta f =$ 1.24 MHz (purple line). When single-cavity short feedback is applied to the laser, a reduction in line width to 391 kHz is observed together with the appearance of noise resonances at multiples of the short-feedback round-trip frequency (green line). For single-cavity long feedback, a further reduction in the line width to 3.8 kHz is measured (blue line). For dual-cavity feedback, Δf amounts to less than 1 kHz (orange line). For both single-cavity feedback configurations the expected noise resonances at the respective round-trip frequencies are visible. In contrast, for dual-cavity feedback only a single but

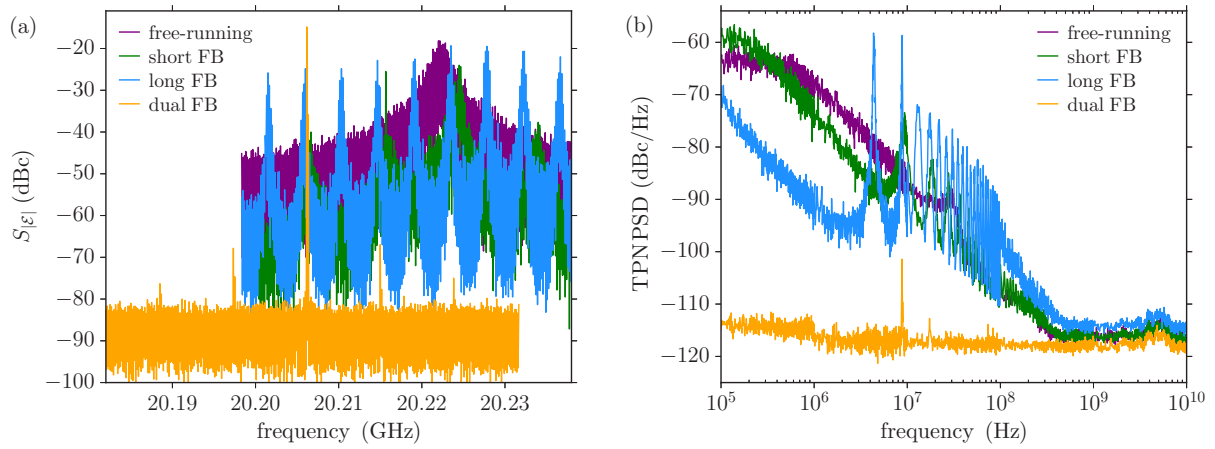

FIG. 11. Experiment: (a) Radio-frequency spectra of the free-running laser (purple), short single-cavity feedback (green), long single-cavity feedback (blue), and dual-cavity feedback (orange). (b) Timing-phase-noise power density spectra corresponding to (a).

highly reduced noise resonance at 9.4 MHz is apparent. The reduction of the noise resonances in the dual-cavity feedback configuration amount to 58 dB at frequencies corresponding to the long cavity and 37 dB for the frequencies corresponding to the short cavity. In Fig. 11(b) the measured timing-phase noise power spectral density is plotted as a function of the offset frequency from the fundamental mode-locked frequency. For the laser without feedback an integrated root-mean-square timing jitter of $\sigma_{\text{rms}} = 1.94$ ps is obtained, corresponding to a σ_{lt} of 13.5 fs. Applying single-cavity short feedback, the timing jitter is increased to $\sigma_{\text{lt}} = 13.8$ fs ($\sigma_{\text{rms}} = 1.98$ ps). This slight increase in the timing jitter is due to the delay length having been optimized for the dual-cavity feedback configuration, since the feedback contribution from the short cavity is very small the delay length is not simultaneously optimized for the single-cavity feedback case (i.e., the total feedback strength effects the repetition rate and hence the resonant feedback delay lengths). For long-cavity feedback a timing-jitter reduction is measured, with a σ_{lt} of 5.2 fs ($\sigma_{\text{rms}} = 739$ fs). For the dual-cavity feedback, we observe a substantially reduced timing jitter, with $\sigma_{\text{lt}} = 0.07$ fs ($\sigma_{\text{rms}} = 10.5$ fs). These results are in agreement with the trends reported in Ref. [29] and with the calculations presented in the previous section.

For these initial experimental results the focus was on timing-jitter reduction and the suppression of the noise-induced feedback cavity resonances. Therefore, in contrast to the simulation results given in Fig. 6, the feedback strength of the long cavity was chosen to be greater than that of the short cavity. The small contribution to the feedback from the short cavity effectively suppresses the resonant oscillations, thereby improving both the short-term and long-term timing stability, as predicted in the previous section.

In the experimental radio frequency and phase noise spectra the feedback resonance side peaks are much larger than in the simulation results. This is because in the experiment the feedback cavities are substantially longer than in the simulations, $\tau_1 \approx 3000\, T_{\text{ISI}}$ compared with $\tau_1 \approx 500\, T_{\text{ISI}}$ (very long delay lengths are impractical to simulated due to long-lived transients) and therefore the noise-induced oscillations are significantly less damped. The shift in the position of the main peak is due to the varying degrees of frequency pulling caused by the single- and dual-cavity feedback configurations [Fig. 11(a)].

V. CONCLUSIONS

The influence of dual-cavity optical feedback on the emission dynamics of a passively mode-locked laser, emitting a pulse train at a repetition rate of 20 GHz, has been numerically investigated. In dependence of the feedback delay times and feedback strength the system exhibits fundamental mode-locking, harmonic mode-locking, quasiperiodic and chaotic dynamics, and feedback-induced satellite pulses. We find a nearly periodic dependence of the dynamics on the two delay times and identify main resonance self-locking regions. We find that the width of the self-locking region increases for longer feedback delay times and that frequency pulling occurs along these regions. Within the self-locking regions fundamental mode-locking occurs and timing-jitter reduction can be achieved. The greatest timing-jitter reduction is found toward the center of the main resonance regions. When both feedback delay lengths are tuned appropriately within the self-locking range, simultaneous timing-jitter reduction and repetition rate tuning is found numerically. Based on the numerical simulations we predict that the repetition rate tuning ranges can be increased with dual-cavity feedback as compared with single-cavity feedback, and that by choosing appropriate resonant feedback delay lengths, improved timing-jitter reduction can be achieved due to the suppression of noise-induced oscillations. The suppression of these oscillations leads to improved timing stability on both short and long timescales in the dual-cavity feedback case.

Initial experimental investigations have been carried out using a dual-cavity setup with two fine-delay tunable external cavity lengths, the results of which are in good agreement with the theoretically predicted trends. Experimentally, a maximum root-mean-square timing-jitter reduction up to a factor of 180 has been found with respect to the free-running laser and up to a factor of 70 as compared to the single long-cavity configuration. A maximum noise resonance reduction of

58 dB, with respect to the single long-cavity case, is observed when both feedback cavities are resonant.

Thus, we state that dual-cavity optical feedback shows great promise for ultranarrow line width, passively mode-locked semiconductor lasers without residual noise resonances at multiples of the external-cavity round-trip frequencies.

ACKNOWLEDGMENTS

L. Jaurigue thanks B. Lingnau and A. Röhm for fruitful discussions and acknowledges support from the GRK 1558 funded by the DFG. The QD laser was manufactured within the EU FP7 (Fast Dot project, Grant No. 224338). S. Breuer acknowledges funding by the Adolf Messer Foundation.

[1] K. Y. Lau, I. Ury, and A. Yariv, Passive and active mode locking of a semiconductor laser without an external cavity, Appl. Phys. Lett. **46**, 1117 (1985).

[2] Steve Sanders, Lars Eng, Joel Paslaski, and A. Yariv, 108 GHz passive mode locking of a multiple quantum well semiconductor laser with an intracavity absorber, Appl. Phys. Lett. **56**, 310 (1990).

[3] O. Solgaard and K. Y. Lau, Optical feedback stabilization of the intensity oscillations in ultrahigh-frequency passively modelocked monolithic quantum-well lasers, IEEE Photonics Technol. Lett. **5**, 1264 (1993).

[4] C.-Y. Lin, F. Grillot, N. A. Naderi, Y. Li, and L. F. Lester, rf linewidth reduction in a quantum dot passively mode-locked laser subject to external optical feedback, Appl. Phys. Lett. **96**, 051118 (2010).

[5] S. Breuer, W. Elsäßer, J. G. McInerney, K. Yvind, J. Pozo, E. A. J. M. Bente, M. Yousefi, A. Villafranca, N. Vogiatzis, and J. Rorison, Investigations of repetition rate stability of a mode-locked quantum dot semiconductor laser in an auxiliary optical fiber cavity, IEEE J. Quantum Electron. **46**, 150 (2010).

[6] D. Arsenijević, A. Schliwa, H. Schmeckebier, M. Stubenrauch, M. Spiegelberg, D. Bimberg, V. Mikhelashvili, and G. Eisenstein, Comparison of dynamic properties of ground- and excited-state emission in p-doped InAs/GaAs quantum-dot lasers, Appl. Phys. Lett. **104**, 181101 (2014).

[7] M. T. Crowley, David Murrell, Nishant Patel, Magnus Breivik, Chang-Yi Lin, Yan Li, Bjorn-Ove Fimland, and L. F. Lester, Analytical modeling of the temperature performance of monolithic passively mode-locked quantum dot lasers, IEEE J. Quantum Electron. **47**, 1059 (2011).

[8] A. G. Vladimirov and D. V. Turaev, Model for passive mode locking in semiconductor lasers, Phys. Rev. A **72**, 033808 (2005).

[9] C. Otto, K. Lüdge, A. G. Vladimirov, M. Wolfrum, and E. Schöll, Delay induced dynamics and jitter reduction of passively mode-locked semiconductor laser subject to optical feedback, New J. Phys. **14**, 113033 (2012).

[10] C. Otto, L. C. Jaurigue, E. Schöll, and K. Lüdge, Optimization of timing jitter reduction by optical feedback for a passively mode-locked laser, IEEE Photon. J. **6**, 1501814 (2014).

[11] U. Keller and Anne C. Tropper, Passively modelocked surface-emitting semiconductor lasers, Phys. Rep. **429**, 67 (2006).

[12] A. S. Pimenov, T. Habruseva, D. Rachinskii, S. P. Hegarty, G. Huyet, and A. G. Vladimirov, The effect of dynamical instability on timing jitter in passively mode-locked quantum-dot lasers, Opt. Lett. **39**, 6815 (2014).

[13] C. Simos, H. Simos, C. Mesaritakis, A. Kapsalis, and D. Syvridis, Pulse and noise properties of a two section passively mode-locked quantum dot laser under long delay feedback, Opt. Commun. **313**, 248 (2014).

[14] L. C. Jaurigue, A. S. Pimenov, D. Rachinskii, E. Schöll, K. Lüdge, and A. G. Vladimirov, Timing jitter of passively mode-locked semiconductor lasers subject to optical feedback: A semi-analytic approach, Phys. Rev. A **92**, 053807 (2015).

[15] E. A. Avrutin, J. H. Marsh, and E. L. Portnoi, Monolithic and multi-gigahertz mode-locked semiconductor lasers: Constructions, experiments, models and applications, IEE Proc. Optoelectron. **147**, 251 (2000).

[16] F. Lelarge, B. Dagens, J. Renaudier, R. Brenot, A. Accard, F. van Dijk, D. Make, O. Le Gouezigou, J. G. Provost, F. Poingt, J. Landreau, O. Drisse, E. Derouin, B. Rousseau, F. Pommereau, and G. H. Duan, Recent advances on InAs/InP quantum dash based semiconductor lasers and optical amplifiers operating at 1.55 μm, IEEE J. Sel. Top. Quantum Electron. **13**, 111 (2007).

[17] K. Lüdge, *Nonlinear Laser Dynamics - From Quantum Dots to Cryptography* (Wiley-VCH, Weinheim, 2012).

[18] M. G. Thompson, D. Larson, A. R. Rae, K. Yvind, R. V Penty, I. H White, J. M. Hvam, A. R. Kovsh, S. S Mikhrin, D. A. Livshits, and I. L. Krestnikov, Monolithic hybrid and passive mode-locked 40-GHz quantum dot laser diodes, *European Conference on Optical Communications* (IEEE, Cannes, France, 2006), pp. 1–2.

[19] N. Rebrova, G. Huyet, D. Rachinskii, and A. G. Vladimirov, Optically injected mode-locked laser, Phys. Rev. E **83**, 066202 (2011).

[20] L. Drzewietzki, S. Breuer, and W. Elsäßer, Timing phase noise reduction of modelocked quantum-dot lasers by time-delayed optoelectronic feedback, Electron. Lett. **49**, 557 (2013).

[21] E. A. Avrutin and B. M. Russell, Dynamics and spectra of monolithic mode-locked laser diodes under external optical feedback, IEEE J. Quantum Electron. **45**, 1456 (2009).

[22] A. G. Vladimirov, D. V. Turaev, and G. Kozyreff, Delay differential equations for mode-locked semiconductor lasers, Opt. Lett. **29**, 1221 (2004).

[23] A. Panchuk, D. P. Rosin, P. Hövel, and E. Schöll, Synchronization of coupled neural oscillators with heterogeneous delays, Int. J. Bifurcation Chaos **23**, 1330039 (2013).

[24] D. C. Lee, Analysis of jitter in phase-locked loops, IEEE Trans. Circuits Syst. II **49**, 704 (2002).

[25] C. Otto, *Dynamics of Quantum Dot Lasers – Effects of Optical Feedback and External Optical Injection*, Springer theses (Springer, Heidelberg, 2014).

[26] S. Gerhard, C. Schilling, F. Gerschütz, M. Fischer, J. Koeth, I. Krestnikov, A. R. Kovsh, M. Kamp, S. Höfling, and A. Forchel, Frequency-dependent linewidth enhancement factor of quantum-dot lasers, IEEE Photonics Technol. Lett. **20**, 1736 (2008).

[27] K. C. Kim, I. K. Han, J. I. Lee, and T. G. Kim, Gain-dependent linewidth enhancement factor in the quantum dot structures, Nanotechnology **21**, 134010 (2010).

[28] Z. J. Jiao, Z. G. Lu, J. R. Liu, P. J. Poole, P. Barrios, D. Poitras, G. Pakulski, J. Caballero, and X. P. Zhang, Linewidth enhancement factor of InAs/InP quantum dot lasers around 1.5 μm, Opt. Commun. **285**, 4372 (2012).

[29] M. Haji, L. Hou, A. E. Kelly, Jehan Akbar, J. H. Marsh, J. M. Arnold, and C. N. Ironside, High frequency optoelectronic oscillators based on the optical feedback of semiconductor mode-locked laser diodes, Opt. Express **20**, 3268 (2012).